Ozone and carbon monoxide budgets over the Eastern Mediterranean

S. Myriokefalitakis [a], N. Daskalakis [a,b,1], G. S. Fanourgakis [a], A. Voulgarakis [c], M. C. Krol [d,e,f], J. M. J. Aan de Brugh [f] and M. Kanakidou [a]

[a] Environmental Chemical Processes Laboratory (ECPL), Department of Chemistry, University of Crete, P.O. Box 2208, 70013 Heraklion, Greece

[b] Institute of Chemical Engineering, Foundation for Research and Technology Hellas (FORTH/ICE - HT), 26504 Patras, Greece

[c] Department of Physics, Imperial College London, London, UK

[d] Meteorology and Air Quality Section, Wageningen University, Wageningen, The Netherlands

[e] Institute for Marine and Atmospheric Research, Utrecht University, Utrecht, The Netherlands

[f] SRON Netherlands Institute for Space Research, Utrecht, The Netherlands

[1] now at: LATMOS, Laboratoire Atmosphères, Milieux, Observations Spatiales, UPMC/UVSQ/CNRS, Paris, France

Corresponding author: stelios@uoc.gr (S. Myriokefalitakis); mariak@uoc.gr (M. Kanakidou)

Abstract

The importance of the long-range transport (LRT) on O_3 and CO budgets over the Eastern Mediterranean has been investigated using the state-of-the-art 3-dimensional global chemistry-transport model TM4-ECPL. A 3-D budget analysis has been performed separating the Eastern from the Western basins and the boundary layer (BL) from the free troposphere (FT). The FT of the Eastern Mediterranean is shown to be a strong receptor of polluted air masses from the Western Mediterranean, and the most important source of polluted air masses for the Eastern Mediterranean BL, with about 40% of O_3 and of CO in the BL to be transported from the FT aloft. Regional anthropogenic sources are found to have relatively small impact on regional air quality in the area, contributing by about 8% and 18% to surface levels of O_3 and CO, respectively. Projections using anthropogenic emissions for the year 2050 but neglecting climate change calculate a surface O_3 decrease of about 11% together with a surface CO increase of roughly 10% in the Eastern Mediterranean.

Keywords: Ozone (O_3), Carbon monoxide (CO), Eastern Mediterranean (EM), Long-range transport (LRT), Free Troposphere (FT)

1. Introduction

Tropospheric O_3 and CO are atmospheric pollutants both generated from natural and anthropogenic sources depending on numerous physical and chemical processes (e.g. Lelieveld and Dentener, 2000). They significantly affect the oxidizing capacity of the troposphere, climate (IPCC, 2013) and human and ecosystem's health (e.g. Jimoda, 2012; Ainsworth et al., 2012; Yue and Unger, 2014). Therefore, much attention is been paid to limit exceedances of threshold air pollution levels set by Environmental policy directives (e.g. DIRECTIVE 2008/50/EC Annex VII). Attribution of air pollution to sources is a prerequisite for designing measures to be taken to comply with such instructions. Pollution within urban agglomerations can build-up both locally (via local emissions and chemistry) and regionally (via transport from other regions) (e.g. Parrish et al., 2011). In the outflow of pollution centers, oxidation of volatile organic compounds (VOCs) and CO fosters the formation of secondary pollutants such as O_3 (Molina and Molina, 2002), which is produced during the oxidation of VOCs in the presence of nitrogen oxides (NO_x) (Crutzen, 1974; Derwent et al., 1996; Monks et al., 2009) following non-linear chemical processes. Therefore, it is particularly important to know whether actions on national level or coordinated actions on regional, or even global scale, are needed to limit air pollution in a region.

In this respect, Colette et al. (2012) analyzed atmospheric pollutant surface observations in Europe to derive trends over the past decade and compared them with multi-model chemistry-transport simulations. They found robust decreases of NO_x throughout Europe except in South-Eastern France and North Italy and pointed out much larger model uncertainty over the Mediterranean than elsewhere. Over the Eastern Mediterranean (EM), they calculate a decrease in non-methane volatile organic compounds (NMVOC) to NO_x ratio indicating a shift in the chemical regime in the area. Beekmann and Vautard (2010) have shown that the Mediterranean atmosphere is a NO_x sensitive regime, while North-Western Europe is always VOC sensitive. Furthermore, modeling studies simulate high O_3 concentrations in the summer, in agreement with the observed northern hemisphere summertime O_3 maxima (Zanis et al., 2014). They also predict higher O_3 levels in parts of the European continent as a result of a warmer climate in the near future (Langner et al., 2012; Zanis et al., 2014) and an increase in regional biogenic emissions, both of which lead to a summertime regional O_3 increase by 1 ppb $^{o}C^{-1}$ (Im et al., 2011). Within large agglomerations of the EM, O_3 is significantly depressed through reaction

64 with NO, followed by HNO_3 formation, in particular during wintertime (Im and Kanakidou,
65 2012).

66 The Mediterranean is among the most climatically sensitive regions of Europe, often exposed to
67 multiple stresses, such as simultaneous water shortage and air pollution exposure (IPCC, 2013).
68 It is also a characteristic region of a strongly coupled atmosphere-ocean system, composed by
69 two basins that differ in air circulation patterns (Millán et al., 2005; Kallos et al., 2007) – the
70 eastern and the western part. EM is affected by several large agglomerations, including the two
71 megacities (http://www.newgeography.com): Istanbul (13.6 M; Turkey) at the northeastern edge,
72 Cairo (17.8 M; Egypt) at the southern edge of the basin, and one agglomeration, Athens, which
73 gathers 40% (4 M) of Greece's total population. The rapid urbanization and the unique location
74 of the EM as a cross-road of air masses affected by various pollution sources has turned air
75 pollution into a challenging environmental problem in the area. Air masses from upwind
76 locations carrying anthropogenic emissions, mainly from Europe, the Balkans and the Black Sea,
77 meet with biomass burning (Sciare et al., 2008), biogenic (Liakakou et al., 2009) and other
78 natural emissions (Gerasopoulos et al., 2011) from surrounding regions under sunny and warm
79 conditions that enhance photochemical build-up of pollutants (Lelieveld et al., 2002; Kanakidou
80 et al., 2011).

81 To quantify the impact of anthropogenic sources on air-quality of the region as the EM, the inter-
82 and the intra- continental transport have to be considered and distinguished from the impact of
83 the regional sources (HTAP, 2011). Such analysis remains challenging, due to the chemical
84 complexity of atmospheric composition and the significant seasonal and interannual variability
85 of meteorological conditions that affect transport patterns (e.g. driven by the North Atlantic
86 Oscillation; Pausata et al., 2012). Thus, large-scale chemistry-transport models (CTMs) are more
87 appropriate tools for studying LRT (e.g. HTAP, 2011) than mesoscale models in which inter-
88 /intra-continental transport procedures are strongly driven by the imposed boundary conditions.
89 Satellite observations of tropospheric O_3, NO_2 and aerosol optical thickness (AOT) over the
90 Mediterranean clearly show the regional tropospheric O_3 column maximum over the
91 Mediterranean sea as well as the high NO_2 columns in the urban pollution centers that surround
92 the basin (Kanakidou et al., 2011). Ground-based and satellite observations and numerical
93 modeling reviewed by Kanakidou et al. (2011) point out that air pollution transported to the area
94 is of similar importance to local sources for the background air pollution levels in the EM.

Indeed, Drori et al. (2012) calculated that transport of air masses from Eastern Europe and Turkey to the EM can contribute up to 50 % of surface CO in the area. Gerasopoulos et al. (2005) analyzing observations provided evidence that the main mechanism controlling the high background tropospheric O_3 levels in the EM is the long-range transport (LRT) from the European continent (mainly during summer) and the local photochemical O_3 build-up (especially under western flow and stagnant wind conditions). In line with these findings, Zanis et al. (2014) attributed the characteristic summertime tropospheric O_3 pool over the EM to enhanced downward transport from the upper troposphere and lower stratosphere that characterize the summertime circulation over this region.

In the present study we investigate the contribution of LRT on O_3 and CO budgets in the Mediterranean basin, using a global CTM, the TM4-ECPL, to conduct a source attribution of atmospheric composition changes. The relative impacts of regional anthropogenic, biomass burning and natural emissions to the air quality in the EM are evaluated. First, the model set-up and methodology followed are described. Then simulated O_3 and CO levels are compared with in-situ observations and satellite retrievals on a European and global level and model deficiencies are discussed. The importance of regional emissions and the strength of LRT for air quality are investigated based on sensitivity simulations and budget analysis. Projected changes resulting from anthropogenic emissions scenarios for 2050 are also discussed.

2. Materials and Methods

2.1 Global Model Set-up

The global CTM TM4-ECPL (Daskalakis et al., 2015 and references therein) is able to simulate oxidant chemistry, accounting for NMVOCs, as well as all major aerosol components, including inorganic aerosols such as sulfate (SO_4^{2-}), nitrate (NO_3^-), ammonium (NH_4^+) using the ISORROPIA II thermodynamic model (Fountoukis and Nenes, 2007) and secondary organic aerosols (SOA). Compared to its parent TM4 model (van Noije et al., 2004), the present version includes a description of glyoxal and other oxygenated organics (Myriokefalitakis et al., 2008) and organic aerosols (Myriokefalitakis et al., 2010). The model also accounts for multiphase chemistry in clouds and aerosol water that affects SOA formation (Myriokefalitakis et al., 2011) and dust solubility (Myriokefalitakis et al., 2015). TM4-ECPL has been previously evaluated for its ability i) to compute atmospheric composition and uncertainties associated with the use of

different biomass burning emissions (Daskalakis et al., 2015), ii) to reproduce distributions of tropospheric O_3 and its precursors, as well as aerosols over Asia in summer 2008 as seen by satellite and by in-situ observations (Quennehen et al., 2015), iii) to simulate the concentrations of sulfate, black carbon (BC) and other aerosols in the Arctic (Eckhardt et al., 2015) and iv) to evaluate the air quality impacts of short-lived pollutants based on current legislation for the recent past and present (Stohl et al., 2015).

For the present study, year 2008 anthropogenic emissions of NMVOC, NO_x, CO, SO_2, NH_3, OC and BC developed within the EU - FP7 ECLIPSE project (Stohl et al., 2015) have been used to drive the chemistry in the model. Methane (CH_4) is calculated by nudging surface concentrations to NOAA flask observations representative of the year of simulation (currently available for the years 1989-2010; M. van Weele, personal communication, 2013). Since TM4-ECPL does not explicitly calculate stratospheric chemistry, upper boundary conditions derived from climatology records of stratospheric concentrations have been applied for O_3, CH_4 and HNO_3. Thus, stratospheric O_3 concentrations are nudged above 50hPa to the concentrations of the year of simulation based on the Multi-Sensor Reanalysis (MSR) climatology record, which is available for the years 1978-2008 (van der A et al., 2010). For stratospheric CH_4 concentrations, the monthly climatology based on the HALogen Occultation Experiment (HALOE) on board the Upper Atmosphere Research Satellite (UARS) (Grooß and Russell III, 2005) is applied above 50 hPa. In the stratosphere, HNO_3 is nudged at 10 hPa using Sub-millimetre and Millimetre Radiometer (SMR) observations from the Odin satellite (Brohede et al., 2008). This approach enables a realistic representation of the concentrations of these compounds in the upper layers of the model and thus of the vertical exchanges between the stratosphere and the troposphere. Further detailed information on the model set up and the emission inventories used in the model is available in Daskalakis et al. (2015).

Here, TM4-ECPL is driven by ECMWF (European Center for Medium - Range Weather Forecasts) Interim re-analysis project (ERA-Interim) meteorology (Dee et al., 2011). Advection of the tracers in the model is parameterized using the slopes scheme (Russell and Lerner, 1981). Convective transport is parameterized based on the Tiedtke (1989) and Olivié (2004) scheme. The vertical diffusion is parameterized as described in Louis (1979). The basic model configuration used for this study (BASE simulation; see Table 1) has a horizontal resolution of 3^o in longitude by 2^o in latitude, 34 vertical hybrid layers from the surface up to 0.1 hPa and a

time-step of 30 min. For this work, all simulations were performed using meteorology for the year 2008. A spin-up of one year (i.e. for the year 2007) with the respective meteorology and emissions has been applied.

2.2 Simulations and Emission Perturbations

A number of simulations have been further performed for this study (Table 1) in order to investigate the importance of LRT over the Mediterranean basin, focusing in particular on the EM part. In short, simulations are performed to investigate the impact of regional anthropogenic (MaskANTHRO), biogenic (MaskBIO) and biomass burning (MaskBB) emissions in the EM. The simulation MaskALL neglects all regional emissions to provide information on the background air-quality levels (sustained by mid - and long - range transport to the EM). Note that for the present work, the area between 15^{o}E - 40^{o}E in longitude and 30^{o}N - 45^{o}N in latitude is defined as the EM domain in the model (i.e. 25 longitudinal boxes and 15 latitudinal boxes for the BASE simulation).

Additionally, simulations are performed to separately investigate the impact of LTR from non-EM parts of Europe (MaskEU), North America (MaskNAM), Asia (MaskAS) and Africa (MaskAF) to the EM background atmosphere. For this work, we use the HTAP phase 2 definitions (available online via the HTAP Wiki-page) for the source regions over which emissions are masked. An additional simulation (FUTURE) investigates the impact of future global anthropogenic emissions on EM O_3 levels, based on emission projections for the year 2050 (Stohl et al., 2015). The sensitivity simulations for the investigation of emissions and LTR strength are performed with the computationally cheaper, coarser horizontal resolution configuration of the model (i.e. 6^{o} in longitude by 4^{o} in latitude).

2.3 Global model evaluation methodology

The model's performance has been evaluated by comparing the simulated O_3 and CO levels with surface observations, ozonesonde data and satellite retrievals, all for the year 2008. O_3 surface observations are taken from the European Monitoring Evaluation Program network (EMEP; www.emep.int) and from the World Ozone and Ultraviolet Radiation Data Centre (WOUDC; http://www.woudc.org) (the location of all surface observational sites used for model evaluation is provided in the supplementary material Table S1 and Fig. S1). Ozonesonde data from sites around the world provided by the WOUDC are used to evaluate the computed vertical structure

of O_3. CO surface observations around the globe for the year 2008 are taken from World Data Centre for Greenhouse Gases (WDCGG; http://ds.data.jma.go.jp/gmd/wdcgg/).

TM4-ECPL results for tropospheric O_3 and CO have been further compared with data from the Tropospheric Emission Spectrometer (TES) satellite instrument. TES is a high resolution (0.1 cm^{-1}), infrared, Fourier Transform spectrometer aboard the NASA Aura satellite that follows a polar Sun - synchronous orbit with an equator crossing time at 01:45 and 13:45 local time, and has a repeating cycle of 16 days. The version 4 of TES global survey data, focusing on the FT region of 800-400 hPa, are used here following the methods presented by Voulgarakis et al. (2011). The TES products are provided in 67 levels in the vertical with a varying layer thickness and with an averaged nadir footprint of 5 km by 8 km (Beer, 2006). Model 3-hourly output is sampled at the times and locations of the TES measurements. The model values are logarithmically interpolated onto the 67 TES pressure levels in the vertical, and the TES a priori profiles and averaging kernels are applied. The processed observational and model data are regridded to a $3^o x2^o$ grid (in longitude by latitude horizontal resolution).

To quantify the model's ability in simulating O_3 and CO levels, statistical parameters commonly used for model validation have been calculated: the correlation coefficient (R), the standard error (STD), the normalized mean bias (NMB), the normalized mean error (NME) and the root mean square error (RMSE). In short, R reflects the strength of the linear relationship between model results and observations (the ability of the model to simulate the observed variability), and it is insensitive to either an additive or a multiplicative factor; STD is a numerical value indicating the reliability of the mean, estimated by the sample standard deviation divided by the square root of the sample size; MNE and MNB indicate the errors and biases towards overestimations; RMSE is a measure of mean relative scatter reflecting both systematic and random errors. All equations used for the statistical analysis of model results are provided in the supplementary material (Eq. S1-S5).

2.4 Budget Calculations

To calculate the pollutant budget, the atmosphere has been divided into three vertical zones; the boundary layer (BL; from the surface up to 850hPa – the 6 first levels of the model), the free troposphere (FT; between 850hPa and the tropopause –the next 13 levels of the model) and the stratosphere (ST; from the tropopause up to the top of the model's atmosphere 0.1hPa – the top

15 levels of the model). Pollutant lateral fluxes through the boundaries of the studied region have been calculated for these three vertical zones as well as vertical exchange fluxes between the BL and the FT and between the FT and the ST. Emissions, chemical production, chemical destruction and deposition have also been computed for the budget analysis. The tropopause in the model is here determined by the lowest grid boxes where monthly mean O_3 concentrations are greater than 150 ppb_v (i.e. the chemical tropopause as in Stevenson et al., 2006). The chemical production of O_3, which occurs through the oxidation of CO, CH_4, and NMVOCs in the presence of NO_x, is here computed as the sum of the change in O_3 concentration due to chemistry (net chemical production) and the O_3 chemical loss computed as the sum of the reactions that destroy O_3. These are O_3 photolysis followed by the reaction of the produced excited oxygen atom with water vapour to form OH radical and O_3 reactions with alkenes, hydrogen peroxy and hydroxyl radicals (for the reactions see Myriokefalitakis et al., 2008). All budget terms are calculated every model time step and averaged/integrated appropriately. Lifetimes are calculated by dividing the burden with the respective loss budget term.

3. Results and discussion

Evaluation of the factors that control surface O_3 and CO levels as reflected in atmospheric air quality modeling is critical for air-quality strategies while an accurate simulation of vertical profiles is important for O_3 climate forcing calculations. In this respect, first the simulated distributions of O_3 and CO for the year 2008 are evaluated and then their budget over the Mediterranean and the impact of specific sources to the surface air pollution levels are discussed.

3.1 Evaluation of O_3 and CO distributions

3.1.1 Evaluation of Surface O_3

To compare observations with model results, EMEP stations have been first divided into four groups, representing different regions of Europe; namely: a) Northwestern Europe ($45^oN – 60^oN$; 10^oW - 15^oE), b) Northeastern Europe (45^oN - 60^oN; 15^oE - 40^oE), c) Southwestern Europe (30^oN - 45^oN; 10^oW - 15^oE) and d) Southeastern Europe (30^oN - 45^oN; 15^oE - 40^oE). Monthly model results are interpolated for each station's coordinates and averaged separately for each group to provide monthly mean surface concentrations of all stations for each of the 4 different European domains (Fig. 1). Note that the number of stations varies between regions and that for

each region the monthly observational data and the respective standard errors as well as model calculations (for every station's coordinates) have been averaged appropriately.

Fig. 1a shows that for the Northwestern European domain, the model overestimates the available observations in summer (R=0.8; MNB=24%). The same pattern is simulated for the Northeastern European domain (Fig. 1b; R=0.9; NMB=27.2%) where the model also overestimates observed O_3 in summer. For both, the Southeastern and the Southwestern parts of Europe (Fig. 1d and Fig. 1c, respectively), TM4-ECPL satisfactory reproduces the observed variability of concentrations (R=0.8) but with a general tendency to overestimate Southwestern Europe surface O_3 in summer (up to 60 ppb_v in summer, NMB=21.8%, while much smaller overestimate is found for Southeastern Europe; NMB=7.5%). However, the general summertime model overestimation of surface O_3 compared to observations implies a potentially strong photochemical O_3 production calculated by the model, especially in the Western part of the Mediterranean, where the model predicts O_3 concentrations for the period from May to September that are higher than the 84.1 percentile ($+1\sigma$, standard deviation) of the measurements (Fig. 1c). These discrepancies can be attributed to the inaccuracies in emissions of O_3 precursors and to the model's coarse resolution that implies limited accuracy of non-linearities in chemistry (Kanakidou and Crutzen, 1999). Another possible reason of the departure of O_3 simulated concentrations from observations during summer is the simulation of the dry deposition O_3 flux.

Simulated surface O_3 is further evaluated on a global scale against available surface observations from the WOUDC, for the year 2008. Fig. S2a presents the point-by-point (scatter plot) of all available measurements from WOUDC and EMEP stations. Observed O_3 mixing ratios are generally well reproduced by the model (R=0.7, RSME = 11.9 ppb_v), but the model in general tends to overestimate the observations (MNB = 15.2%).

3.1.2 Evaluation of O_3 vertical structure

Ozonesonde observations compiled by the WOUDC have also been used to evaluate the models' capability in reproducing the O_3 observed vertical profiles. Fig. 2 presents the comparison of model results with observations in 2008 at the Hohenpeissenberg (Germany) and Payerne (Switzerland) ozonesonde stations for five pressure levels (900 hPa, 800 hPa, 500 hPa, 400 hPa and 200 hPa), covering boundary layer and the low and high free troposphere. In order to compare with the WOUDC observations, both the model results and the ozonesondes

observations have been firstly linearly interpolated into layers of 50 hPa from the surface to the top of the atmosphere. Comparisons for the other European stations available by WOUDC (i.e. Lindenber – Germany; Legiovo – Poland; De Bilt – The Netherlands; Ankara – Turkey) are further presented in the supplementary material (Fig. S3). The model captures the O_3 distribution quite well almost at all sites throughout the lower troposphere. Differences in the model performance at the various stations can be due to the different characteristics of the stations, for instance the O_3 precursor source regions, the intensity of photochemistry and the major transport patterns that are affecting them. Above 200hPa model overestimations are mainly attributed to the upper boundary conditions applied in the model (see Section 2.1). The point-by-point comparison of monthly mean values for all WOUDC ozonesonde tropospheric observations sites for the year 2008 (2344 pairs) is also presented in Fig. S2b. Globally, the model overestimates observations by roughly 20% (R = 0.8, NMB = 10.6%, NME 20%). Similar performance is also found over Europe (Fig. S2b).

3.1.3 Evaluation of Free Tropospheric O_3 Concentrations

Simulated O_3 concentrations are further compared to the TES satellite retrievals for the middle/low FT. Fig. 3a depicts the annual mean calculated O_3 concentrations between 800 and 400 hPa (the vertical region with the maximum TES instrument sensitivity) over Europe calculated by TM4-ECPL and Fig. 3c shows the percentage difference from TES retrievals. The model tends to overestimate the mean free tropospheric O_3 concentrations retrieved from TES observations over Northern Europe and Scandinavia (up to 3%), while simulated O_3 concentrations are underestimated up to 5% in the EM.

Fig. S4 also shows the seasonality in the zonal mean (60^oS – 60^oN) O_3 concentrations in the free troposphere (800 - 400hPa) as computed by the model and its difference from the TES observations. This comparison reveals an O_3 overestimate by the model (up to about 10%) in the northern high latitude regions during the summer months and an underestimate in lower latitudes that reaches 15% in the tropics during NH spring-summer. However, it is worth to note here that the disagreement between TM4-ECPL and TES could be partially explained by the observed TES positive bias between 3-10 ppbv (Nassar et al., 2008).

303 *3.1.4 Evaluation of surface CO concentrations*

304 TM4-ECPL results have also been compared with surface CO observations from the WDCGG
305 database for the year 2008. Fig. 4 presents the CO comparison of monthly mean model results
306 with observations for countries within Europe; although the number of the CO monitoring
307 stations is limited (8 stations for the year 2008 over Europe). For this comparison, monthly
308 model results have been extracted for each station and an average for all stations in the same
309 country has been obtained. Fig. 4 shows that the model satisfactory simulates the CO surface
310 concentrations for Germany (R = 0.7, NMB= -4.9%), Slovenia (R = 0.6, NMB = -2.8%) and
311 Switzerland (R = 0.6, NMB = -3.3%), while an offset is found for the station in The Netherlands
312 (R = 0.9, NMB= -26.6%). The model evaluation for all CO surface observational sites over
313 Europe and the globe for the year 2008 is also presented in Fig. S2c, based on monthly mean
314 values. The point-by-point global comparison shows that the model generally underestimates the
315 observations (NMB = -21%) but captures the variability (R = 0.9).

316 *3.1.5 Evaluation of Free Tropospheric CO concentrations*

317 Simulated CO concentrations in the lower free troposphere are also compared with the TES
318 products. Fig. 3b depicts the annual mean CO concentrations between 800-400 hPa over Europe
319 calculated by TM4-ECPL and Fig. 3d shows the percentage difference between the model results
320 and the CO TES product for 2008. The model underestimates the annual mean CO
321 concentrations over Europe by about 10%. The seasonality of the zonal mean CO concentrations
322 between 60^{o}S and 60^{o}N in the middle/low free troposphere (800-400hPa) as calculated by TM4-
323 ECPL is presented in Fig. S4b. The model calculates a winter and a spring maximum in the
324 Northern Hemisphere (NH), and less than half concentrations in the Southern Hemisphere.
325 Secondary maxima due to biomass burning processes are also simulated for the tropics from
326 August to February. The model tends to underestimate CO summer concentrations in the NH . In
327 the NH subtropics (0^{o} – 30^{o}N) the model underestimation of CO concentrations reaches almost
328 20% from April to late June (Fig. S4d). On the contrary, the model tends to overestimate the
329 retrieved CO tropospheric concentrations by about 10% in the mid-latitudes from September to
330 December. Note however, that studies of TES CO products validation against aircraft data have
331 shown a small bias of TES products that was slightly negative (<10 %) in mid-latitudes and
332 slightly positive (<10 %) in the tropics (Luo et al., 2007; Lopez et al., 2008). Thus, some TM4-
333 ECPL disagreement (Fig. S4f) can be attributed to observational errors. The tendency to

underestimate northern extratropical CO and to overestimate tropical CO in the free troposphere is, however, a common feature in current atmospheric modelling (e.g. Naik et al., 2013).

3.2 Tropospheric budget analysis for O_3 and CO

3.2.1 Global troposphere

Global tropospheric burden for O_3 and CO governed by both sources (i.e., the chemical production and the stratosphere-troposphere exchanges for O_3, and emissions and chemical production for CO) and sinks (chemical destruction and deposition for both O_3 and CO) have been calculated for the year 2008. Large O_3 chemical production (5294 Tg yr^{-1}) and chemical destruction (5031 Tg yr^{-1}) terms are calculated, while dry deposition flux (753 Tg yr^{-1}) and stratospheric net influx (490 Tg yr^{-1}) are computed to be an order of magnitude lower. These values are well in the range of the 26 model results that participated in the Stevenson et al. (2006) model intercomparison study for the year 2000 (chemical production of 5110 ± 606 Tg yr^{-1}, a chemical destruction of 4668 ± 727 Tg yr^{-1}, a dry deposition flux of 1003 ± 200 Tg yr^{-1} and a stratospheric influx of 552 ± 200 Tg yr^{-1}). Similarly, the mean tropospheric O_3 burden of 345 Tg here calculated is close to the 344 ± 39 Tg O_3 tropospheric burden derived by Stevenson et al. (2006).

For the year 2008 in the TM4-ECPL, global CO primary emissions amount 896 Tg yr^{-1}, global CO chemical production is calculated to be 1946 Tg yr^{-1} that is about twice the primary emissions and chemical destruction to be 2647 Tg yr^{-1}. The total CO source (i.e. emissions and chemical production, 2427 Tg yr^{-1} for 2008) is in agreement with earlier studies; e.g. about 2760 Tg yr^{-1} for the year 1997 derived by Müller and Stavrakou (2005) using inverse modeling calculated the global CO source and 2455 Tg yr^{-1} calculated by Kanakidou and Crutzen (1999). The chemical destruction of CO in the model is due to the oxidation by OH radicals. OH radical oxidation is also the primary loss mechanism for methane (CH_4) and for this OH atmospheric burden is commonly studied simultaneously to CH_4 chemical lifetime. For the year 2008, the TM4-ECPL calculates a tropospheric chemical lifetime of CH_4 of about 8.1 years, which is close to the low-end of mean tropospheric chemical CH_4 lifetime due to OH oxidation for the year 2000, as derived from the ACCMIP (Atmospheric Chemistry and Climate Modeling Intercomparison Project) multi-model mean (9.8 ± 1.6 yr; Voulgarakis et al., 2013). CO tropospheric burden calculated by TM4-ECPL is 317 Tg for the year 2008, similar to the

364 estimate by Kanakidou and Crutzen (1999) and by 20% lower than the 397 Tg calculated by
365 Müller and Stavrakou (2005). However, the dry deposition sink calculated both by Bergamaschi
366 et al. (2000) (288 Tg yr^{-1}) and by Müller and Stavrakou (2005) (186-205 Tg yr^{-1}) is larger than
367 the deposition flux of about 172 Tg yr^{-1} calculated by TM4-ECPL.

368 *3.2.2 Eastern Mediterranean*

369 Fig. 5 and Fig. 6 sketch the budget calculations over the Mediterranean, for O_3 and for CO
370 respectively, separating also the Western from the Eastern basin (shaded/non - shaded areas) and
371 the BL (lower parts) from the FT (upper parts). For the BASE simulation, in the EM-BL O_3 is
372 imported from the North (5 Tg yr^{-1}), from the western boundary (20 Tg yr^{-1}) and from the EM-
373 FT aloft (36 Tg yr^{-1}) and exported mainly to the South (38 Tg yr^{-1}) and to the East (24 Tg yr^{-1}).
374 This result further indicates the significance of free tropospheric O_3 intrusions for the EM O_3
375 abundance in the BL. Photochemistry in the EM-BL (involving NO_x, VOCs photo-oxidation)
376 acts as an additional significant source for O_3 in the region with a net chemical production
377 calculated to about 12 Tg yr^{-1}. For CO, the model calculates for the EM-BL a burden of 0.6 Tg of
378 CO, a chemical production of 10 Tg yr^{-1}, primary emissions in the region of 8 Tg yr^{-1} and a dry
379 deposition flux of 3 Tg yr^{-1}. Free-tropospheric intrusion imports 22 Tg yr^{-1} of CO to the EM-BL
380 and 20 Tg yr^{-1} of CO are advected from the west. The model also calculates a strong CO outflow
381 of 32 Tg yr^{-1} to the South and a weaker import from the northern boundary that accounts about 6
382 Tg yr^{-1}.

383 As far as it concerns the EM-FT (Fig. 5 and Fig. 6; upper parts), significant amounts of O_3 and
384 CO are advected through the western boundary (383 Tg yr^{-1} and 228 Tg yr^{-1}, respectively) and
385 even larger amounts are exported due to chemical build-up and LRT to the East (445 Tg yr^{-1} and
386 240 Tg yr^{-1}, respectively). Three times higher O_3 burden over the EM (2.1 Tg) is simulated in the
387 FT than the BL, while O_3 residence time over the EM is calculated to be about 2.7 days in the BL
388 and about 1.5 days in the FT. The model simulates a net O_3 photochemical source of 3 Tg yr^{-1}
389 and a CO net chemical destruction of about 4 Tg yr^{-1} in the EM-FT. Subsidence from higher
390 atmospheric layers is an important source for both O_3 (48 Tg yr^{-1}) and CO (12 Tg yr^{-1}) in the
391 EM-FT. Moreover, northern winds enriched in O_3 and CO carry significant amounts of these
392 pollutants to the region's FT (39 Tg yr^{-1} and 25 Tg yr^{-1}, respectively), while about 17 Tg yr^{-1} of
393 O_3 are also imported from the southern boundary to the EM-FT, partly resulting from transport
394 from Asia and Africa (17% and 16% respectively).

3.2.3 Western Mediterranean and comparison to the Eastern basin

Fig. 5 and Fig. 6 (shaded area) also depict O_3 and CO budgets in the Western Mediterranean (WM). TM4-ECPL calculates a significant influence from the surroundings since advection of pollutants into the WM-FT (sum of all import terms) is about 2 orders of magnitude higher than the net photochemical source in this region.

The WM-BL is receiving 4 times lower amounts of O_3 from the FT (9 Tg yr^{-1}) than the Eastern basin, and the chemical production of O_3 (36 Tg yr^{-1}) is slightly lower than that for EM. According to TM4-ECPL model calculations, stratospheric O_3 intrusions are an important source (75 Tg yr^{-1}) of tropospheric O_3 over the entire Mediterranean. However, over the WM smaller O_3 amounts are computed (roughly 36% of the total stratospheric intrusions), due to the stagnant conditions in the BL (Millán et al., 2005) as compared to the EM, even though an O_3 burden of about 2.1 Tg in the WM-FT is also calculated as for the case of EM-FT. In the WM-BL, the O_3 chemical lifetime is calculated to be about 12.7 days while the overall residence time in the western basin is estimated at about 4.7 days (i.e. about 33% longer than that in the EM) due to deposition and fast outflow. Ventilation by advection is about 3 times faster in the EM than in the WM (about 4 days versus 12 days, respectively). However, the chemical lifetime of O_3 in the BL is almost identical in the two basins (about 12 days) while the subsidence from the FT is about 4 times higher in the EM than in the WM. Overall, the EM-BL is acting as a receptor of O_3 of air masses mainly from the FT (59%) and the WM (33%), as well as a source of O_3 and CO for the downwind locations to the South (60%) and the East (40%). Air-masses advected from the North are about 2 times richer in O_3 in the WM-FT than in the EM-FT, even though the subsidence from the stratosphere provides about 78% more O_3 in the EM-FT than in the WM-FT.

3.3 Contribution of sources to air pollution

TM4-ECPL calculations show that the Mediterranean (Fig. 7c) is among the regions experiencing the highest surface O_3 concentrations in the globe together with eastern U.S. and Central Asia (Fig. 7a). In general, TM4-ECPL calculates high surface O_3 concentrations in the mid-latitudes of the NH, over regions with high anthropogenic activity (US, Europe and China) as well as in the tropical areas affected by biomass burning emissions (Fig. 7a). The zonal mean distribution of O_3 concentrations (not shown) presents enhanced values in the sub-tropics

425 because of O_3 production in regions affected by biomass burning such as Central Africa. The
426 model also calculates high O_3 concentrations in the pollution plumes over the Atlantic and the
427 outflow over Japan.

428 Simulated surface CO also shows enhanced concentrations over polluted regions of the NH (i.e.
429 US, Europe and China) as well as the biomass burning peaks over Central Africa and the
430 Amazon Basin (Fig. 7b). Although, primary CO sources are mainly from anthropogenic origin
431 (roughly 60%), CO secondary sources from VOC oxidation are calculated to be by 70% from
432 CH_4 and by 30% from NMVOCs (e.g. Poisson et al., 2000). The CO zonal mean distribution (not
433 shown) clearly shows the high NH concentrations, resulting from both high primary and
434 secondary sources north of 30^{o}S. TM4-ECPL calculates higher CO concentrations in the winter
435 (not shown) mainly due to the lower loss by reaction with OH that presents a seasonal wintertime
436 minimum in the troposphere (reduced oxidizing capacity).

437 In order to investigate the contribution of local and distant sources to air pollution in the BL,
438 emission perturbation simulations have been performed and compared to the base case
439 simulation (BASE) as previously explained in Section 2.2. Percent differences were calculated as
440 100*(BASE-MaskX)/BASE; where MaskX is the respective sensitivity simulation as presented
441 in Table 1.

442 *3.3.1 O_3 surface concentrations*

443 The model (BASE) calculates a surface annual O_3 mean mixing ratio of about 43 ppb_v over the
444 European domain in the model (Fig. 7c), with a maximum exceeding 55 ppb_v over the central
445 and Eastern Mediterranean. The calculations attribute up to 15% of the O_3 surface concentrations
446 to the regional anthropogenic emissions in the EM (MaskAnthro vs. BASE), with an annual
447 mean contribution in the EM of about 8% (Fig. 8a). Additionally, up to 5% on an annual basis is
448 associated with biogenic emissions (MaskBIO vs. BASE), but less than 1% is due to biomass
449 burning emissions (MaskBB vs. BASE). All regional emissions accounted by the model
450 (MaskALL vs. BASE) are responsible for about 11% of O_3 surface levels on annual base, with a
451 maximum contribution of 18% over and south of the Levantine Sea (Fig. 8c), indicating thus the
452 importance of air-mass transport from neighboring regions (i.e. LRT by advection and
453 subsidence to the region). When European emissions are neglected (MaskEU vs. BASE), the
454 model calculates about 13% of reduction in O_3 surface concentrations over the EM (Fig. S5a).

Northern America's emissions (Fig. S5b) affect the surface O_3 concentrations over the entire European continent by about 5% (MaskNAM vs. BASE). Asian emissions (MaskAS vs. BASE) affect O_3 surface concentrations by 10% on annual basis (Fig. S5c), while the African continent's emissions (MaskAF vs. BASE) contribute about 4% to EM basin surface O_3 concentrations (Fig. S5d).

3.3.2 CO surface concentrations

For CO concentrations over Europe, the model calculates a surface annual mean mixing ratio of 110 ppb_v, with a maximum concentration of 128 ppb_v over EM (Fig. 7d). Anthropogenic local emissions in the EM contribute by 18% to the surface CO levels in the EM (Fig. 8b) annually. Maximum anthropogenic contribution (roughly 32%) to surface CO concentrations is calculated over Cairo. On the other hand, CO concentrations over the EM are associated by about 9% on annual basis with regional biogenic VOC oxidation (not shown) and about 3% are due to biomass burning emissions (not shown). All regional emissions accounted by the model (Fig. 8d) are responsible for 23% of CO surface levels, while the remaining could be attributed to LRT. On an annual basis, European emissions (MaskEU) contribute by about 25% to the calculated CO surface concentrations over the EM (Fig. S6a), Northern America's emissions (MaskNAM) by 12% (Fig. S6b), Asian emissions (MaskAS) by 26% (Fig. S6c) and African emissions (MaskAF) by 11% (Fig. S6d).

3.4 Projected changes due to anthropogenic emissions

In Fig. 8e and 8f, the simulation using anthropogenic emissions as projected for the year 2050 (FUTURE) is compared to the BASE (i.e. 100x(FUTURE-BASE)/BASE). A 16% increase in surface O_3 over central Europe is due to the reduction in NO_x anthropogenic emissions (a reduction in the NO_x O_3-titration effect), while a decrease in surface O_3 by about 11% is calculated for the Mediterranean (Fig. 8e) is due to the reduction in O_3 chemical formation and to import/export fluxes changes. On the opposite, CO surface concentrations are calculated to decrease by about 10% over central Europe. This change is the overall effect of the decrease (more than 40%) in the primary anthropogenic emissions, an almost similar in magnitude increase in the OH radical concentrations (affecting both the secondary CO source and the chemical sink of CO) and changes in the transport fluxes. The opposite trend is projected for the EM, where an increase (Fig. 8f) by about 10% in CO surface concentrations is computed. This

485 change reflects mainly the increase of CO primary anthropogenic emissions in the south
486 combined with a reduction in surface OH levels by about 20% (e.g. due to smaller precursor O_3
487 concentrations) that leads to a reduction in both the secondary source and in the chemical sink of
488 CO in the EM.

489 All FUTURE O_3 imports compared to the BASE simulation (computed as [100x(FUTURE-
490 BASE)/BASE]) due to advection to EM-BL are calculated to decrease roughly by 13% on
491 average, with the Northern boundaries imports to decrease, however, by about 17%. On the other
492 hand, exports from the EM-BL are also calculated to decrease under 2050 anthropogenic
493 emissions, mainly to the South (14%). Note that the same decrease is also calculated for the EM-
494 FT, resulting thus to a decrease in downdraft to EM-BL of about 13%. As far as it concerns the
495 CO, in the EM-BL increases in CO imports from the EM-FT boundary and from the West (about
496 24% and 17%, respectively) are calculated. In contrast, a decrease in import from the North of
497 about 14% is also calculated for EM-BL, which can also be attributed to impact of Asian
498 emissions as discussed in the previous section (Section 3.3.2). CO has a longer lifetime
499 compared to O_3, which makes the LRT Asian contribution to European pollution more
500 pronounced on CO than on O_3 within Europe (i.e. Fig. S6c). For the FUTURE simulation, both
501 meteorology and CH_4 concentrations are kept constant in the model, thus the increase in CO
502 chemical production and destruction is attributed to the respective increase in O_3 levels and thus
503 in OH production, leading to a more aggressive CO loss. As explained in section 2.1 changes in
504 meteorology and the stratospheric boundary conditions, which may occur in the future under
505 climate change, are not taken into account by the model. Thus, the computed anti-correlation
506 between O_3 and CO future changes over the EM is driven by the changes in anthropogenic
507 emissions and the induced differences in the oxidation capacity.

508 **4. Conclusions**

509 The global chemistry-transport model TM4-ECPL is able to reproduce observations of O_3 and
510 CO at the surface, the BL and in FT in the rural and remote atmosphere over Europe. This
511 allowed us to analyze the O_3 and CO budget over the EM. We found that the EM atmosphere is
512 strongly affected by air masses from surrounding regions and thus by sources other than local.
513 Similar conclusions for the EM, documented in different ways, have been reached by other
514 modeling studies (e.g. Im and Kanakidou, 2012; Zanis et al., 2014) as well as in the reviews by
515 Kanakidou et al. (2011) and Kallos et al. (2013) and references therein. In the present study we

516 further quantified the contribution of various sources to the O_3 and CO budget in the EM. In
517 particular, our calculations show that local anthropogenic emissions are responsible for about 8%
518 of surface O_3 concentration and 18% of CO surface concentrations, while downward transport
519 from the FT provides about 38% of O_3 sources and about 33% of CO sources into the EM-BL
520 and horizontal advection from the surrounding regions contributes by about 51% and 27%,
521 respectively. Therefore, neglecting all the emissions in the EM region (i.e. anthropogenic,
522 biomass burning, biogenic and natural emissions) leads to a reduction in annual mean surface
523 concentrations of only 11% in O_3 and of 23% in CO.

524 For anthropogenic emissions projected for the year 2050, the model calculates a reduction of
525 about 11% in the regional O_3 surface concentrations, with a contemporaneous increase in CO
526 surface concentrations of roughly 10% in the EM. The opposite changes of O_3 and CO due to
527 future anthropogenic emissions could be attributed to the respective changes of oxidation
528 capacity within the EM and to changes in the fluxes in and out the EM which are driven by
529 large-scale concentration changes. However, our calculations do not account for potential
530 changes in meteorology and stratospheric boundary conditions. Overall, this work indicates that
531 O_3 and CO surface levels in the EM are mainly driven by LRT of pollution and related
532 precursors within the BL, but also through the FT and subsequent downdraft to the BL. This
533 implies that mitigation of local anthropogenic emissions is not sufficient for significant
534 improvements in air quality in the Mediterranean region, and that coordinated efforts between
535 the countries surrounding and located upwind of the basin are required.
536

Acknowledgements

This work has been initiated in the frame of the CityZEN project (megaCITY - Zoom for the Environment, FP7-ENV-2008-212095) and has been finalized with support to SM and GSF by ECLIPSE (Evaluating the CLimate and Air Quality ImPacts of Short-livEd Pollutants, FP7-ENV-2011-282688) and to ND by PEGASOS (Pan - European Gas - AeroSOls - climate interaction Study, FP7-ENV-2010-265148) collaborative projects funded by the European Commission. We thank Prof. N. Mihalopoulos and Dr. G. Kouvarakis for Finokalia station data availability and the World Ozone and Ultraviolet Radiation Data Centre (WOUDC) for ozonesondes data availability.

References

Ainsworth, E.A., Yendrek, C.R., Sitch, S., Collins, W.J., Emberson, L.D., 2012. The effects of tropospheric ozone on net primary productivity and implications for climate change. Annu. Rev. Plant Biol. 63, 637–61. doi:10.1146/annurev-arplant-042110-103829

Beekmann, M., Vautard, R., 2010. A modelling study of photochemical regimes over Europe: Robustness and variability. Atmos. Chem. Phys. 10, 10067–10084. doi:10.5194/acp-10-10067-2010

Beer, R., 2006. TES on the aura mission: scientific objectives, measurements, and analysis overview. IEEE Trans. Geosci. Remote Sens. 44, 1102–1105. doi:10.1109/TGRS.2005.863716

Bergamaschi, P., Hein, R., Heimann, M., Crutzen, P.J., 2000. Inverse modeling of the global CO cycle: 1. Inversion of CO mixing ratios. J. Geophys. Res. 105, 1909. doi:10.1029/1999jd900818

Brohede, S., McLinden, C.A., Urban, J., Haley, C.S., Jonsson, A.I., Murtagh, D., 2008. Odin stratospheric proxy NO_y measurements and climatology. Atmos. Chem. Phys. 8, 5731–5754. doi:10.5194/acp-8-5731-2008

Colette, A., Granier, C., Hodnebrog, Ø., Jakobs, H., Maurizi, A., Nyiri, A., Rao, S., Amann, M., Bessagnet, B., D'Angiola, A., Gauss, M., Heyes, C., Klimont, Z., Meleux, F., Memmesheimer, M., Mieville, A., Rouil, L., Russo, F., Schucht, S., Simpson, D., Stordal, F., Tampieri, F., Vrac, M., 2012. Future air quality in Europe: a multi-model assessment of projected exposure to ozone. Atmos. Chem. Phys. 12, 10613–10630. doi:10.5194/acp-12-10613-2012

Crutzen, P.J., 1974. Photochemical reactions initiated by and influencing ozone in unpolluted tropospheric air. Tellus 26, 47–57. doi:10.1111/j.2153-3490.1974.tb01951.x

Daskalakis, N., Myriokefalitakis, S., Kanakidou, M., 2015. Sensitivity of tropospheric loads and lifetimes of short lived. Atmos. Chem. Phys. 15, 3543–3563. doi:10.5194/acp-15-3543-2015

Dee, D.P., Uppala, S.M., Simmons, A.J., Berrisford, P., Poli, P., Kobayashi, S., Andrae, U., Balmaseda, M.A., Balsamo, G., Bauer, P., Bechtold, P., Beljaars, A.C.M., van de Berg, L., Bidlot, J., Bormann, N., Delsol, C., Dragani, R., Fuentes, M., Geer, A.J., Haimberger, L., Healy, S.B., Hersbach, H., Hólm, E. V, Isaksen, L., Kållberg, P., Köhler, M., Matricardi, M., McNally, A.P., Monge-Sanz, B.M., Morcrette, J.J., Park, B.K., Peubey, C., de Rosnay, P., Tavolato, C., Thépaut, J.N., Vitart, F., 2011. The ERA-Interim reanalysis: configuration and performance of the data assimilation system. Q. J. Roy. Meteor. Soc. 137, 553–597. doi:10.1002/qj.828

Derwent, R.G., Jenkin, M.E., Saunders, S.M., 1996. Photochemical ozone creation potentials for a large number of reactive hydrocarbons under European conditions. Atmos. Environ. 30, 181–199. doi:10.1016/1352-2310(95)00303-G

Drori, R., Dayan, U., Edwards, D.P., Emmons, L.K., Erlick, C., 2012. Attributing and quantifying carbon monoxide sources affecting the Eastern Mediterranean: a combined satellite, modelling, and synoptic analysis study. Atmos. Chem. Phys. 12, 1067–1082. doi:10.5194/acp-12-1067-2012

Eckhardt, S., Quennehen, B., Olivié, D.J.L., Berntsen, T.K., Cherian, R., Christensen, J.H.,

590 Collins, W., Crepinsek, S., Daskalakis, N., Flanner, M., Herber, A., Heyes, C., Hodnebrog,
591 Ø., Huang, L., Kanakidou, M., Klimont, Z., Langner, J., Law, K.S., Lund, M.T., Mahmood,
592 R., Massling, A., Myriokefalitakis, S., Nielsen, I.E., Nøjgaard, J.K., Quaas, J., Quinn, P.K.,
593 Raut, J.-C., Rumbold, S.T., Schulz, M., Sharma, S., Skeie, R.B., Skov, H., Uttal, T., Salzen,
594 K. von, Stohl, A., 2015. Current model capabilities for simulating black carbon and sulfate
595 concentrations in the Arctic atmosphere: a multi-model evaluation using a comprehensive
596 measurement data set. Atmos. Chem. Phys. 15, 9413–9433. doi:doi:10.5194/acp-15-9413-
597 2015

598 Fountoukis, C., Nenes, A., 2007. ISORROPIA II: a computationally efficient thermodynamic
599 equilibrium model for K+ -Ca2+-Mg2+- NH4+ - Na+- SO42- - NO3- - Cl- - H2O aerosols.
600 Atmos. Chem. Phys. 7, 4639–4659. doi:10.5194/acp-7-4639-2007

601 Gerasopoulos, E., Amiridis, V., Kazadzis, S., Kokkalis, P., Eleftheratos, K., Andreae, M.O.,
602 Andreae, T.W., El-Askary, H., Zerefos, C.S., 2011. Three-year ground based measurements
603 of aerosol optical depth over the Eastern Mediterranean: the urban environment of Athens.
604 Atmos. Chem. Phys. 11, 2145–2159. doi:10.5194/acp-11-2145-2011

605 Gerasopoulos, E., Kouvarakis, G., Vrekoussis, M., Kanakidou, M., Mihalopoulos, N., 2005.
606 Ozone variability in the marine boundary layer of the eastern Mediterranean based on 7-
607 year observations. J. Geophys. Res. D Atmos. 110, 1–12. doi:10.1029/2005JD005991

608 Grooß, J.U., Russell III, J.M., 2005. Technical note: A stratospheric climatology for O3, H2O,
609 CH4, NOx, HCl and HF derived from HALOE measurements. Atmos. Chem. Phys. 5,
610 2797–2807. doi:10.5194/acp-5-2797-2005

611 HTAP, T., 2011. Hemispheric Transport of Air Pollution 2010 Part A: Ozone And Particulate
612 Matter. Air Pollut. Stud.

613 Im, U., Kanakidou, M., 2012. Impacts of East Mediterranean megacity emissions on air quality.
614 Atmos. Chem. Phys. 12, 6335–6355. doi:10.5194/acp-12-6335-2012

615 Im, U., Markakis, K., Poupkou, A., Melas, D., Unal, A., Gerasopoulos, E., Daskalakis, N.,
616 Kindap, T., Kanakidou, M., 2011. The impact of temperature changes on summer time
617 ozone and its precursors in the Eastern Mediterranean. Atmos. Chem. Phys. 11, 3847–3864.
618 doi:10.5194/acp-11-3847-2011

619 Jimoda, L., 2012. Effects of particulate matter on human health, the ecosystem, climate and
620 materials: A review. Facta Univ. Work. Living … 9, 27–44.

621 Kallos, G., Astitha, M., Katsafados, P., Spyrou, C., 2007. Long-Range Transport of
622 Anthropogenically and Naturally Produced Particulate Matter in the Mediterranean and
623 North Atlantic: Current State of Knowledge. J. Appl. Meteorol. Climatol. 46, 1230–1251.
624 doi:10.1175/JAM2530.1

625 Kallos, G., Mitsakou, C., Alastuey, A., van Aardenne, J., Astitha, M., Cusack, M., Doering, U.,
626 Gerasopoulos, E., Hatzianastassiou, N., Kanakidou, M., Kushta, J., Lelieveld, J., Levin, Z.,
627 Mihalopoulos, N., Millán, M., Palau, J.L., Perez, N., Pey, J., Querol, X., Solomos, S.,
628 Spyrou, C., Theodosi, C., Zerefos, C., 2013. Mechanisms of Climate Variability, Air
629 Quality and Impacts of Atmospheric Constituents in the Mediterranean Region, in: Navarra,
630 A., Tubiana, L. (Eds.), Advances in Global Change Research. Springer Netherlands,
631 Dordrecht, pp. 119–156. doi:10.1007/978-94-007-5781-3_4

632 Kanakidou, M., Crutzen, P.J., 1999. The photochemical source of carbon monoxide: Importance,

633 uncertainties and feedbacks. Chemosph. - Glob. Chang. Sci. 1, 91–109.
634 doi:http://dx.doi.org/10.1016/S1465-9972(99)00022-7

635 Kanakidou, M., Mihalopoulos, N., Kindap, T., Im, U., Vrekoussis, M., Gerasopoulos, E.,
636 Dermitzaki, E., Unal, A., Koçak, M., Markakis, K., Melas, D., Kouvarakis, G., Youssef,
637 A.F., Richter, A., Hatzianastassiou, N., Hilboll, A., Ebojie, F., Wittrock, F., von Savigny,
638 C., Burrows, J.P., Ladstaetter-Weissenmayer, A., Moubasher, H., 2011. Megacities as hot
639 spots of air pollution in the East Mediterranean. Atmos. Environ. 45, 1223–1235.
640 doi:10.1016/j.atmosenv.2010.11.048

641 Kanakidou, M., Singh, H.B., Valentin, K.M., Crutzen, P.J., 1991. A two-dimensional study of
642 ethane and propane oxidation in the troposphere. J. Geophys. Res. 96, 15395–15413.
643 doi:10.1029/91jd01345

644 Langner, J., Engardt, M., Baklanov, A., Christensen, J.H., Gauss, M., Geels, C., Hedegaard,
645 G.B., Nuterman, R., Simpson, D., Soares, J., Sofiev, M., Wind, P., Zakey, A., 2012. A
646 multi-model study of impacts of climate change on surface ozone in Europe. Atmos. Chem.
647 Phys. 12, 10423–10440. doi:10.5194/acp-12-10423-2012

648 Lelieveld, J., Berresheim, H., Borrmann, S., Crutzen, P.J., Dentener, F.J., Fischer, H., Feichter,
649 J., Flatau, P.J., Heland, J., Holzinger, R., Korrmann, R., Lawrence, M.G., Levin, Z.,
650 Markowicz, K.M., Mihalopoulos, N., Minikin, A., Ramanathan, V., De Reus, M., Roelofs,
651 G.J., Scheeren, H. a, Sciare, J., Schlager, H., Schultz, M., Siegmund, P., Steil, B.,
652 Stephanou, E.G., Stier, P., Traub, M., Warneke, C., Williams, J., Ziereis, H., 2002. Global
653 air pollution crossroads over the Mediterranean. Science 298, 794–9.
654 doi:10.1126/science.1075457

655 Lelieveld, J., Dentener, F.J., 2000. What controls tropospheric ozone? J. Geophys. Res. 105,
656 3531. doi:10.1029/1999JD901011

657 Liakakou, E., Bonsang, B., Williams, J., Kalivitis, N., Kanakidou, M., Mihalopoulos, N., 2009.
658 C2–C8 NMHCs over the Eastern Mediterranean: Seasonal variation and impact on regional
659 oxidation chemistry. Atmos. Environ. 43, 5611–5621. doi:10.1016/j.atmosenv.2009.07.067

660 Lopez, J.P., Luo, M., Christensen, L.E., Loewenstein, M., Jost, H., Webster, C.R., Osterman, G.,
661 2008. TES carbon monoxide validation during two AVE campaigns using the Argus and
662 ALIAS instruments on NASA's WB-57F. J. Geophys. Res. 113, D16S47.
663 doi:10.1029/2007JD008811

664 Louis, J.-F., 1979. A parametric model of vertical eddy fluxes in the atmosphere. Boundary-
665 Layer Meteorol. 17, 187–202. doi:10.1007/BF00117978

666 Luo, M., Rinsland, C., Fisher, B., Sachse, G., Diskin, G., Logan, J., Worden, H., Kulawik, S.,
667 Osterman, G., Eldering, A., Herman, R., Shephard, M., 2007. TES carbon monoxide
668 validation with DACOM aircraft measurements during INTEX-B 2006. J. Geophys. Res.
669 112, D24S48. doi:10.1029/2007JD008803

670 Millán, M., Estrela, M., Sanz, M., 2005. Climatic feedbacks and desertification: the
671 Mediterranean model. J. … 684–701.

672 Molina, L.T., Molina, M.J. (Eds.), 2002. Air Quality in the Mexico Megacity, Alliance for
673 Global Sustainability Bookseries. Springer Netherlands, Dordrecht. doi:10.1007/978-94-
674 010-0454-1

675 Monks, P.S., Granier, C., Fuzzi, S., Stohl, A., Williams, M.L., Akimoto, H., Amann, M.,

Baklanov, A., Baltensperger, U., Bey, I., Blake, N., Blake, R.S., Carslaw, K., Cooper, O.R., Dentener, F., Fowler, D., Fragkou, E., Frost, G.J., Generoso, S., Ginoux, P., Grewe, V., Guenther, A., Hansson, H.C., Henne, S., Hjorth, J., Hofzumahaus, A., Huntrieser, H., Isaksen, I.S.A., Jenkin, M.E., Kaiser, J., Kanakidou, M., Klimont, Z., Kulmala, M., Laj, P., Lawrence, M.G., Lee, J.D., Liousse, C., Maione, M., McFiggans, G., Metzger, A., Mieville, A., Moussiopoulos, N., Orlando, J.J., O'Dowd, C.D., Palmer, P.I., Parrish, D.D., Petzold, A., Platt, U., Pöschl, U., Prévôt, A.S.H., Reeves, C.E., Reimann, S., Rudich, Y., Sellegri, K., Steinbrecher, R., Simpson, D., ten Brink, H., Theloke, J., van der Werf, G.R., Vautard, R., Vestreng, V., Vlachokostas, C., von Glasow, R., 2009. Atmospheric composition change – global and regional air quality. Atmos. Environ. 43, 5268–5350. doi:10.1016/j.atmosenv.2009.08.021

Müller, J.-F., Stavrakou, T., 2005. Inversion of CO and NO_x emissions using the adjoint of the IMAGES model. Atmos. Chem. Phys. 5, 1157–1186. doi:10.5194/acp-5-1157-2005

Myriokefalitakis, S., Daskalakis, N., Mihalopoulos, N., Baker, A.R., Nenes, A., Kanakidou, M., 2015. Changes in dissolved iron deposition to the oceans driven by human activity: a 3-D global modelling study. Biogeosciences 12, 3973–3992. doi:10.5194/bg-12-3973-2015

Myriokefalitakis, S., Tsigaridis, K., Mihalopoulos, N., Sciare, J., Nenes, A., Kawamura, K., Segers, A., Kanakidou, M., 2011. In-cloud oxalate formation in the global troposphere: a 3-D modeling study. Atmos. Chem. Phys. 11, 5761–5782. doi:10.5194/acp-11-5761-2011

Myriokefalitakis, S., Vignati, E., Tsigaridis, K., Papadimas, C., Sciare, J., Mihalopoulos, N., Facchini, M.C., Rinaldi, M., Dentener, F.J., Ceburnis, D., Hatzianastasiou, N., O'Dowd, C.D., van Weele, M., Kanakidou, M., 2010. Global Modeling of the Oceanic Source of Organic Aerosols. Adv. Meteorol. 2010, 1–16. doi:10.1155/2010/939171

Myriokefalitakis, S., Vrekoussis, M., Tsigaridis, K., Wittrock, F., Richter, A., Brühl, C., Volkamer, R., Burrows, J.P., Kanakidou, M., 2008. The influence of natural and anthropogenic secondary sources on the glyoxal global distribution. Atmos. Chem. Phys. Discuss. 8, 1673–1708. doi:10.5194/acpd-8-1673-2008

Naik, V., Voulgarakis, A., Fiore, A.M., Horowitz, L.W., Lamarque, J.-F., Lin, M., Prather, M.J., Young, P.J., Bergmann, D., Cameron-Smith, P.J., Cionni, I., Collins, W.J., Dalsøren, S.B., Doherty, R., Eyring, V., Faluvegi, G., Folberth, G.A., Josse, B., Lee, Y.H., MacKenzie, I.A., Nagashima, T., van Noije, T.P.C., Plummer, D.A., Righi, M., Rumbold, S.T., Skeie, R., Shindell, D.T., Stevenson, D.S., Strode, S., Sudo, K., Szopa, S., Zeng, G., 2013. Preindustrial to present-day changes in tropospheric hydroxyl radical and methane lifetime from the Atmospheric Chemistry and Climate Model Intercomparison Project (ACCMIP). Atmos. Chem. Phys. 13, 5277–5298. doi:10.5194/acp-13-5277-2013

Nassar, R., Logan, J.A., Worden, H.M., Megretskaia, I.A., Bowman, K.W., Osterman, G.B., Thompson, A.M., Tarasick, D.W., Austin, S., Claude, H., Dubey, M.K., Hocking, W.K., Johnson, B.J., Joseph, E., Merrill, J., Morris, G.A., Newchurch, M., Oltmans, S.J., Posny, F., Schmidlin, F.J., Vömel, H., Whiteman, D.N., Witte, J.C., 2008. Validation of Tropospheric Emission Spectrometer (TES) nadir ozone profiles using ozonesonde measurements. J. Geophys. Res. 113, D15S17. doi:10.1029/2007JD008819

Olivié, D.J.L., 2004. Comparison between archived and off-line diagnosed convective mass fluxes in the chemistry transport model TM3. J. Geophys. Res. 109, D11303. doi:10.1029/2003JD004036

720 Parrish, D.D., Singh, H.B., Molina, L., Madronich, S., 2011. Air quality progress in North
721 American megacities: A review. Atmos. Environ. 45, 7015–7025.
722 doi:10.1016/j.atmosenv.2011.09.039

723 Pausata, F.S.R., Pozzoli, L., Vignati, E., Dentener, F.J., 2012. North Atlantic Oscillation and
724 tropospheric ozone variability in Europe: model analysis and measurements
725 intercomparison. Atmos. Chem. Phys. 12, 6357–6376. doi:10.5194/acp-12-6357-2012

726 Poisson, N., Kanakidou, M., Crutzen, P., 2000. Impact of Non-Methane Hydrocarbons on
727 Tropospheric Chemistry and the Oxidizing Power of the Global Troposphere: 3-
728 Dimensional Modelling Results. J. Atmos. Chem. 36, 157–230.
729 doi:10.1023/A:1006300616544

730 Quennehen, B., Raut, J.-C., Law, K.S., Ancellet, G., Clerbaux, C., Kim, S.-W., Lund, M.T.,
731 Myhre, G., Olivié, D.J.L., Safieddine, S., Skeie, R.B., Thomas, J.L., Tsyro, S., Bazureau,
732 A., Bellouin, N., Daskalakis, N., Hu, M., Kanakidou, M., Klimont, Z., Kupiainen, K.,
733 Myriokefalitakis, S., Quaas, J., Rumbold, S.T., Schulz, M., Cherian, R., Shimizu, A., Wang,
734 J., Yoon, S.-C., Zhu, T., 2015. Multi-model evaluation of short-lived pollutant distributions
735 over East Asia during summer 2008. Atmos. Chem. Phys. Discuss. 15, 11049–11109.
736 doi:10.5194/acpd-15-11049-2015

737 Russell, G.L., Lerner, J.A., 1981. A New Finite-Differencing Scheme for the Tracer Transport
738 Equation. J. Appl. Meteorol. 20, 1483–1498. doi:10.1175/1520-
739 0450(1981)020<1483:ANFDSF>2.0.CO;2

740 Sciare, J., Oikonomou, K., Favez, O., Liakakou, E., Markaki, Z., Cachier, H., Mihalopoulos, N.,
741 2008. Long-term measurements of carbonaceous aerosols in the Eastern Mediterranean:
742 evidence of long-range transport of biomass burning. Atmos. Chem. Phys. 8, 5551–5563.
743 doi:10.5194/acp-8-5551-2008

744 Stevenson, D.S., Dentener, F.J., Schultz, M.G., Ellingsen, K., van Noije, T.P.C., Wild, O., Zeng,
745 G., Amann, M., Atherton, C.S., Bell, N., Bergmann, D.J., Bey, I., Butler, T., Cofala, J.,
746 Collins, W.J., Derwent, R.G., Doherty, R.M., Drevet, J., Eskes, H.J., Fiore, a. M., Gauss,
747 M., Hauglustaine, D. a., Horowitz, L.W., Isaksen, I.S. a., Krol, M.C., Lamarque, J.-F.F.,
748 Lawrence, M.G., Montanaro, V., Müller, J.-F.F., Pitari, G., Prather, M.J., Pyle, J. a., Rast,
749 S., Rodriguez, J.M., Sanderson, M.G., Savage, N.H., Shindell, D.T., Strahan, S.E., Sudo,
750 K., Szopa, S., 2006. Multimodel ensemble simulations of present-day and near-future
751 tropospheric ozone. J. Geophys. Res. 111, D08301. doi:10.1029/2005jd006338

752 Stohl, A., Aamaas, B., Amann, M., Baker, L.H., Bellouin, N., Berntsen, T.K., Boucher, O.,
753 Cherian, R., Collins, W., Daskalakis, N., Dusinska, M., Eckhardt, S., Fuglestvedt, J.S.,
754 Harju, M., Heyes, C., Hodnebrog, Ø., Hao, J., Im, U., Kanakidou, M., Klimont, Z.,
755 Kupiainen, K., Law, K.S., Lund, M.T., Maas, R., MacIntosh, C.R., Myhre, G.,
756 Myriokefalitakis, S., Olivié, D., Quaas, J., Quennehen, B., Raut, J.-C., Rumbold, S.T.,
757 Samset, B.H., Schulz, M., Seland, Ø., Shine, K.P., Skeie, R.B., Wang, S., Yttri, K.E., Zhu,
758 T., 2015. Evaluating the climate and air quality impacts of short-lived pollutants. Atmos.
759 Chem. Phys. Discuss. 15, 15155–15241. doi:doi:10.5194/acpd-15-15155-2015

760 Tiedtke, M., 1989. A Comprehensive Mass Flux Scheme for Cumulus Parameterization in
761 Large-Scale Models. Mon. Weather Rev. 117, 1779–1800. doi:10.1175/1520-
762 0493(1989)117<1779:ACMFSF>2.0.CO;2

763 van der A, R.J., Allaart, M. a. F., Eskes, H.J., 2010. Multi sensor reanalysis of total ozone.

764 Atmos. Chem. Phys. 10, 11277–11294. doi:10.5194/acp-10-11277-2010

765 van Noije, T.P.C., Eskes, H.J., van Weele, M., van Velthoven, P.F.J., 2004. Implications of the
766 enhanced Brewer-Dobson circulation in European Centre for Medium-Range Weather
767 Forecasts reanalysis ERA-40 for the stratosphere-troposphere exchange of ozone in global
768 chemistry transport models. J. Geophys. Res. 109, D19308. doi:10.1029/2004JD004586

769 Voulgarakis, A., Naik, V., Lamarque, J.-F., Shindell, D.T., Young, P.J., Prather, M.J., Wild, O.,
770 Field, R.D., Bergmann, D., Cameron-Smith, P., Cionni, I., Collins, W.J., Dalsøren, S.B.,
771 Doherty, R.M., Eyring, V., Faluvegi, G., Folberth, G.A., Horowitz, L.W., Josse, B.,
772 MacKenzie, I.A., Nagashima, T., Plummer, D.A., Righi, M., Rumbold, S.T., Stevenson,
773 D.S., Strode, S. a., Sudo, K., Szopa, S., Zeng, G., 2013. Analysis of present day and future
774 OH and methane lifetime in the ACCMIP simulations. Atmos. Chem. Phys. 13, 2563–2587.
775 doi:10.5194/acp-13-2563-2013

776 Voulgarakis, A., Telford, P.J., Aghedo, a. M., Braesicke, P., Faluvegi, G., Abraham, N.L.,
777 Bowman, K.W., Pyle, J. a., Shindell, D.T., 2011. Global multi-year O3-CO correlation
778 patterns from models and TES satellite observations. Atmos. Chem. Phys. 11, 5819–5838.
779 doi:10.5194/acp-11-5819-2011

780 Yue, X., Unger, N., 2014. Ozone vegetation damage effects on gross primary productivity in the
781 United States. Atmos. Chem. Phys. 14, 9137–9153. doi:10.5194/acp-14-9137-2014

782 Zanis, P., Hadjinicolaou, P., Pozzer, A., Tyrlis, E., Dafka, S., Mihalopoulos, N., Lelieveld, J.,
783 2014. Summertime free-tropospheric ozone pool over the eastern Mediterranean/Middle
784 East. Atmos. Chem. Phys. 14, 115–132. doi:10.5194/acp-14-115-2014

785

786

787 **Table 1.** Outline of simulations performed for this study.

Simulation	Description
BASE	The base case simulation for the year 2008.
MaskANTRO	Neglecting the anthropogenic emissions in the Eastern Mediterranean domain.
MaskBB	Neglecting the biomass burning emissions in the Eastern Mediterranean domain.
MaskBIO	Neglecting the biogenic emissions in the Eastern Mediterranean domain.
MaskALL	Neglecting the anthropogenic, biomass burning and biogenic emissions in the Eastern Mediterranean domain.
MaskEU	Neglecting all emissions over Europe.
MaskNAM	Neglecting all emissions over Northern America.
MaskAS	Neglecting all emissions over Asia.
MaskAF	Neglecting all emissions over Africa.
FUTURE	Taking into account projected anthropogenic emission of the year 2050.

788

789

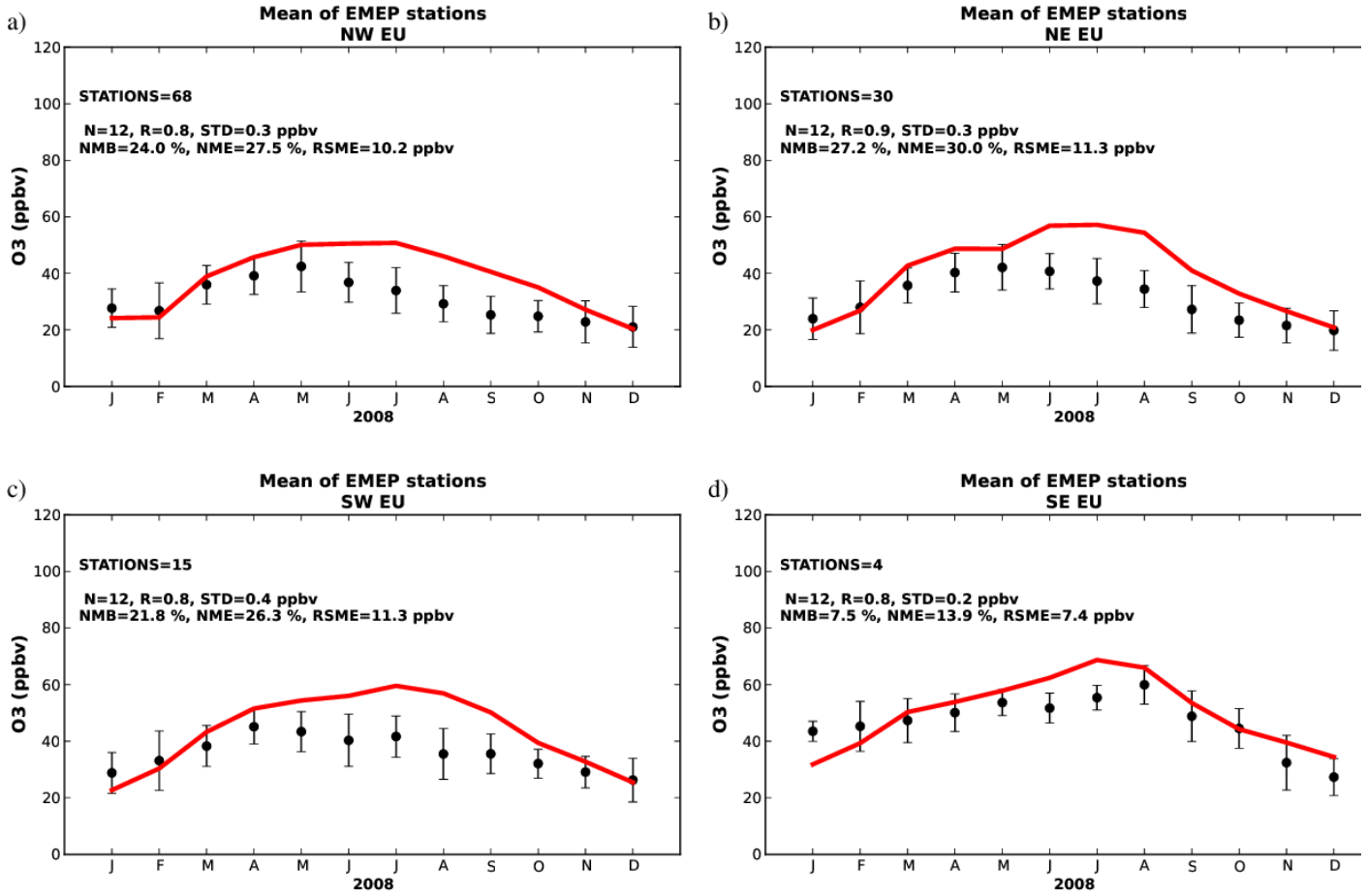

Fig. 1. Comparison of O_3 levels (ppb_v) from TM4-ECPL BASE simulation (red lines) with surface monthly mean observations from EMEP stations (black dots) and the respective standard deviation of the observed O_3 levels (ppb_v) (with black vertical lines) at a) NW Europe, b) NE Europe, c) SW Europe and d) SE Europe.

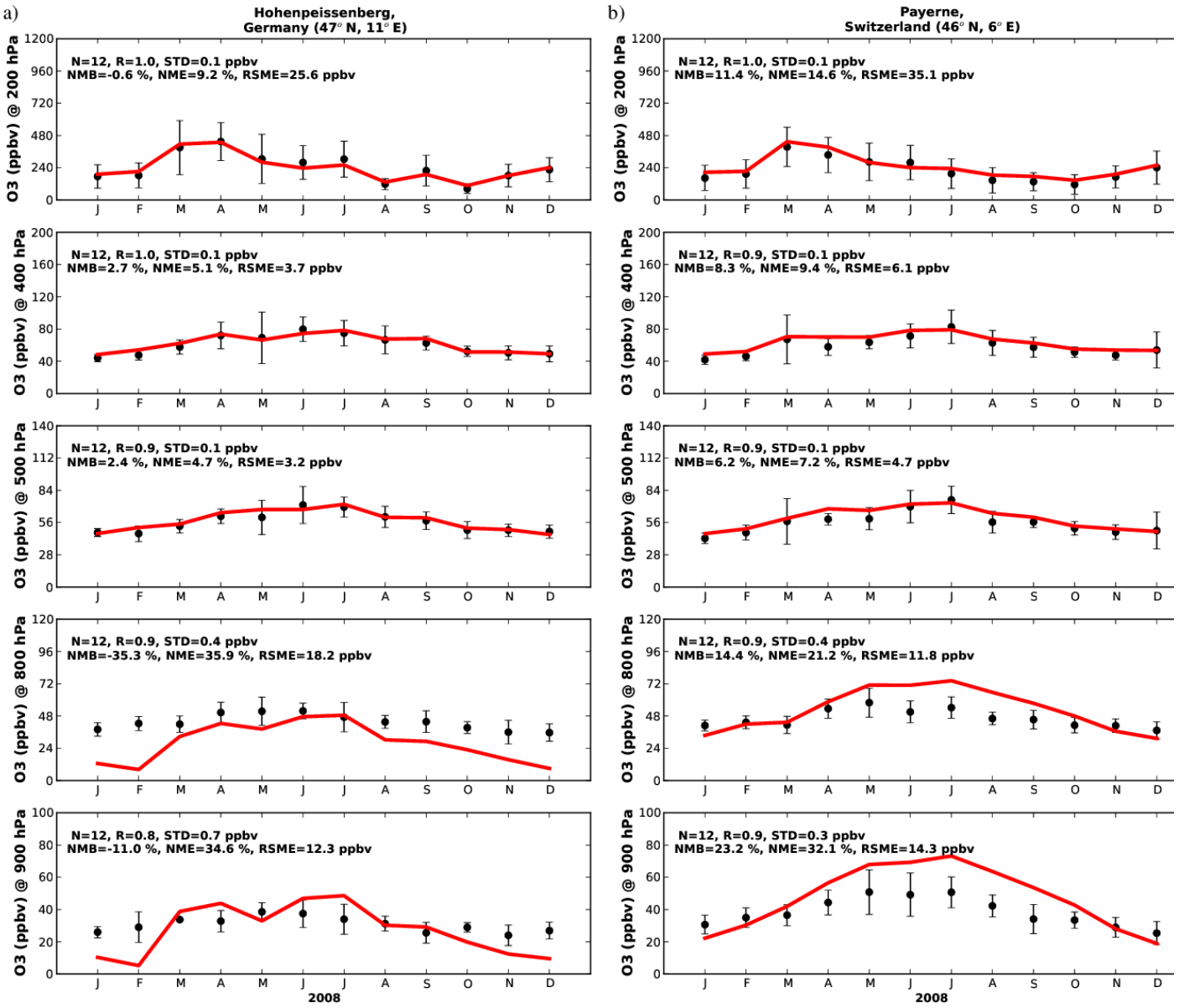

Fig. 2. Comparison of O_3 levels (ppb_v) from TM4-ECPL BASE simulation (red line) with O_3 sonde station data (black dots, mean and standard deviation) at five pressure levels (900; 800; 500; 400; 200 hPa) for two WOUDC stations: a) Hohenpeissenberg, Germany (47°N, 11E°); b) Payerne, Switzerland (46°N, 6°E) (see additional comparisons at other European stations in Fig. S3 in the supplementary material).

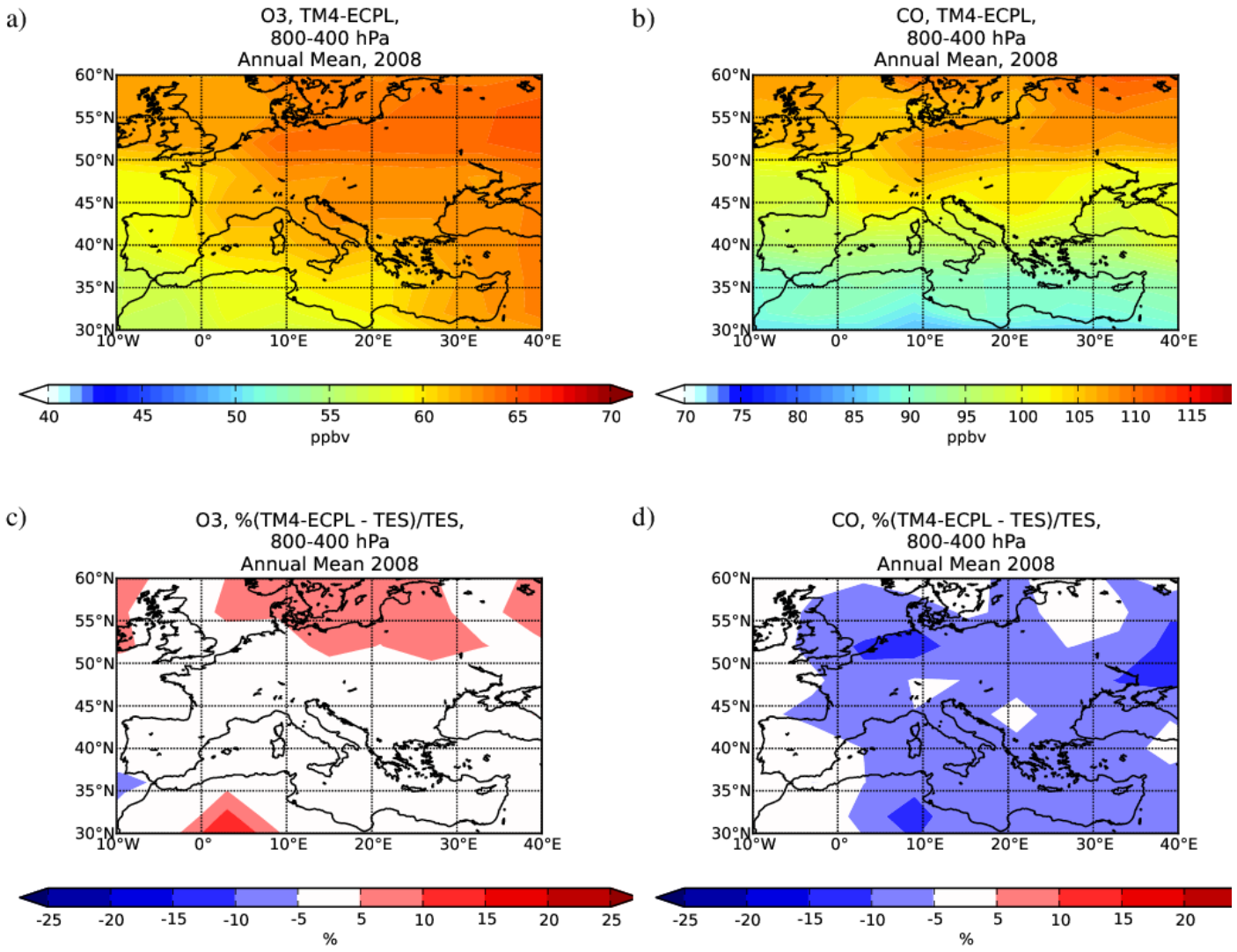

803
804 **Fig. 3.** Simulated annual mean free tropospheric concentrations (ppb_v) in the 800-400 hPa zone
805 over Europe for a) O_3, b) CO, and the percentage difference of TM4-ECPL BASE simulation
806 results from TES retrieved concentrations [100 x (BASE-TES)/TES] for c) O_3 and d) CO in the
807 same zone.

808

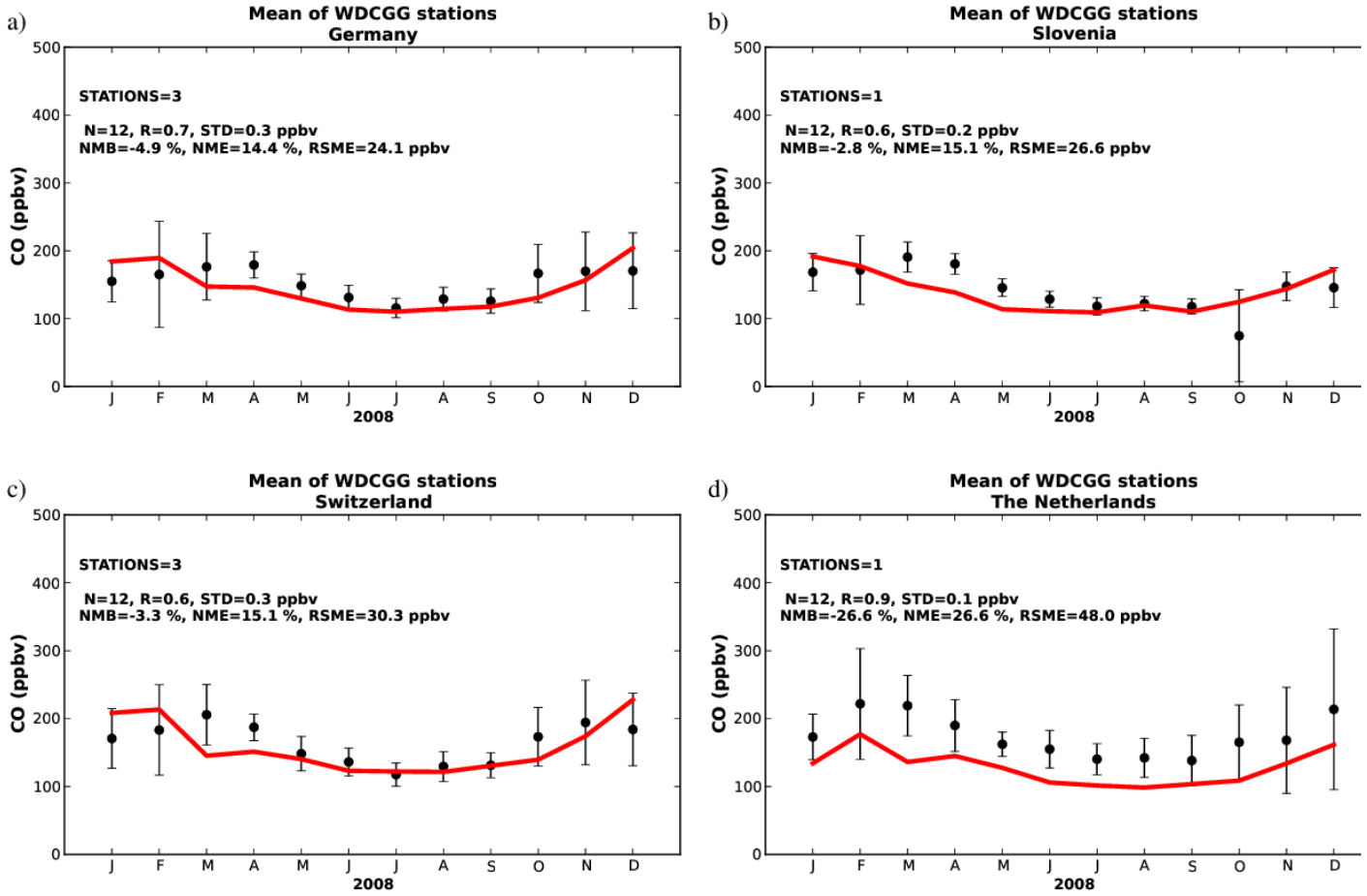

Fig. 4. Comparison of surface CO levels (ppb_v) calculated by TM4-ECPL BASE simulation (red line) with observations (monthly mean values for WDCGG stations, black dots, mean and standard deviation) at a) Germany, b) Slovenia c) Switzerland and d) The Netherlands

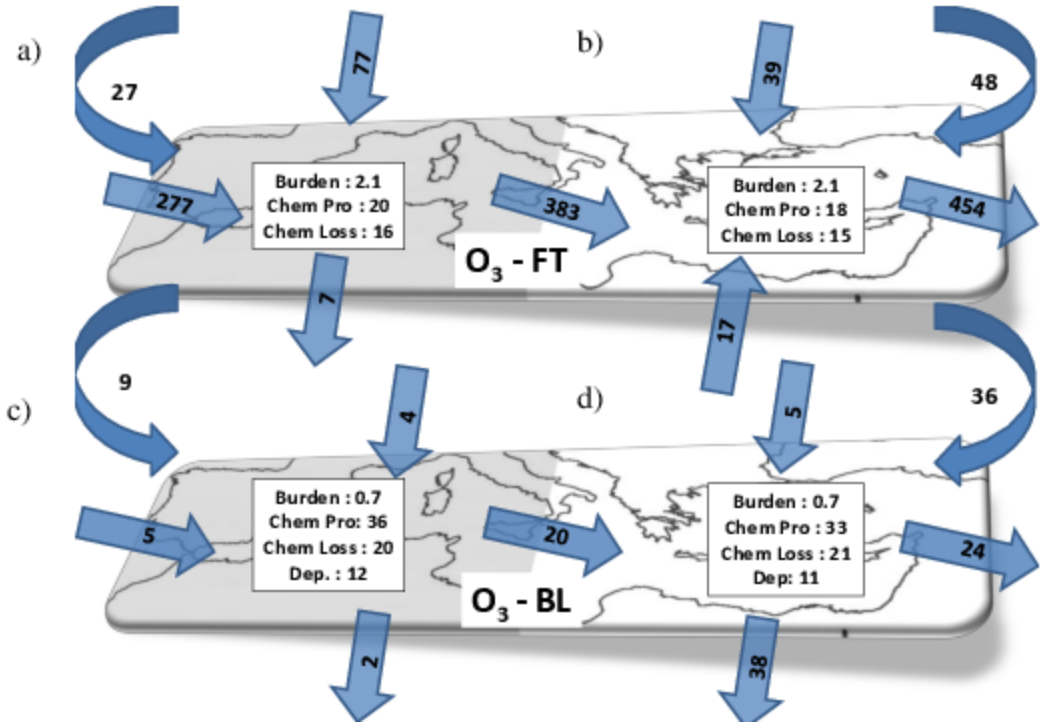

Fig. 5. O_3 annual (2008; BASE simulation) budget analysis for Western (a,c; shaded area) and Eastern Mediterranean (b,d; non-shaded area) for a,b) the free troposphere (FT; upper figure) and c,d) the boundary layer (BL; bottom figure) including the burden, the chemistry, the deposition and the fluxes at each boundary. All budget terms and fluxes (Tg yr^{-1}) are annual totals; burdens (Tg) are annual averages. Straight arrows indicate N-S and W-E advection fluxes, while curved arrows indicate vertical fluxes from the upper troposphere to the FT and from the FT to the BL.

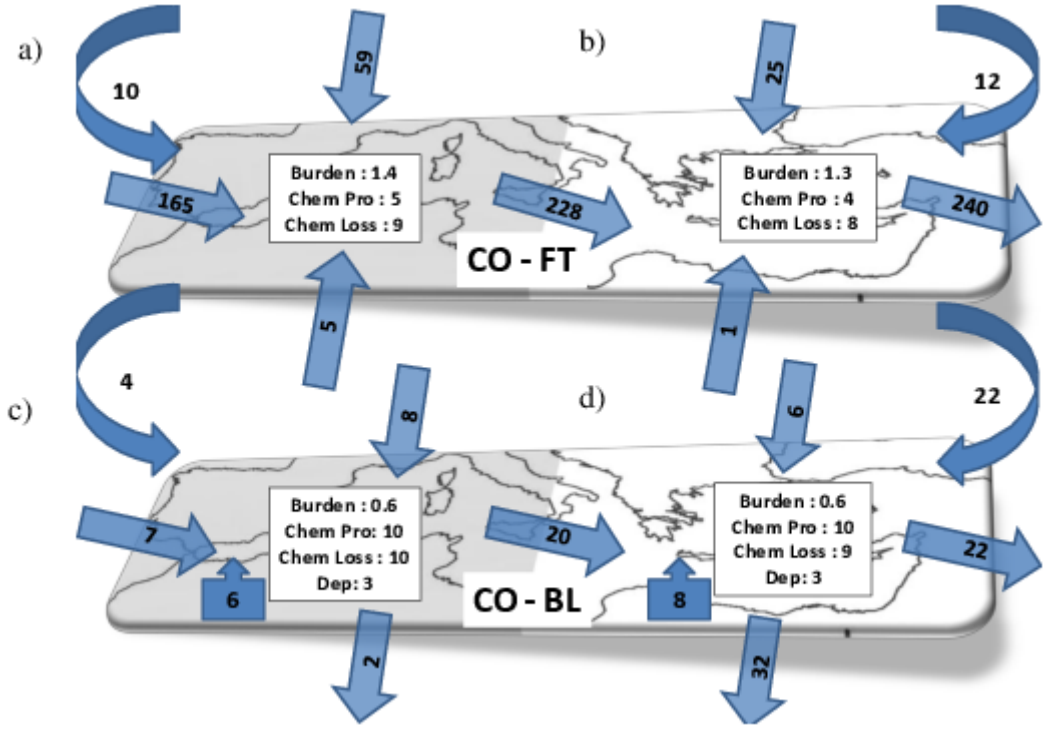

Fig. 6. CO annual (2008; BASE simulation) budget analysis for Western (a,c; shaded area) and Eastern Mediterranean (b,d; non-shaded area) for a,b) the free troposphere (FT; upper figure) and c,d) the boundary layer (BL; bottom figure) including the burden, the emissions, the chemistry, the deposition and the fluxes at each boundary.. Straight arrows indicate N-S and W-E advection fluxes, curved arrows indicate vertical fluxes from the upper troposphere to the FT and from the FT to the BL and box-arrows indicate CO emissions.

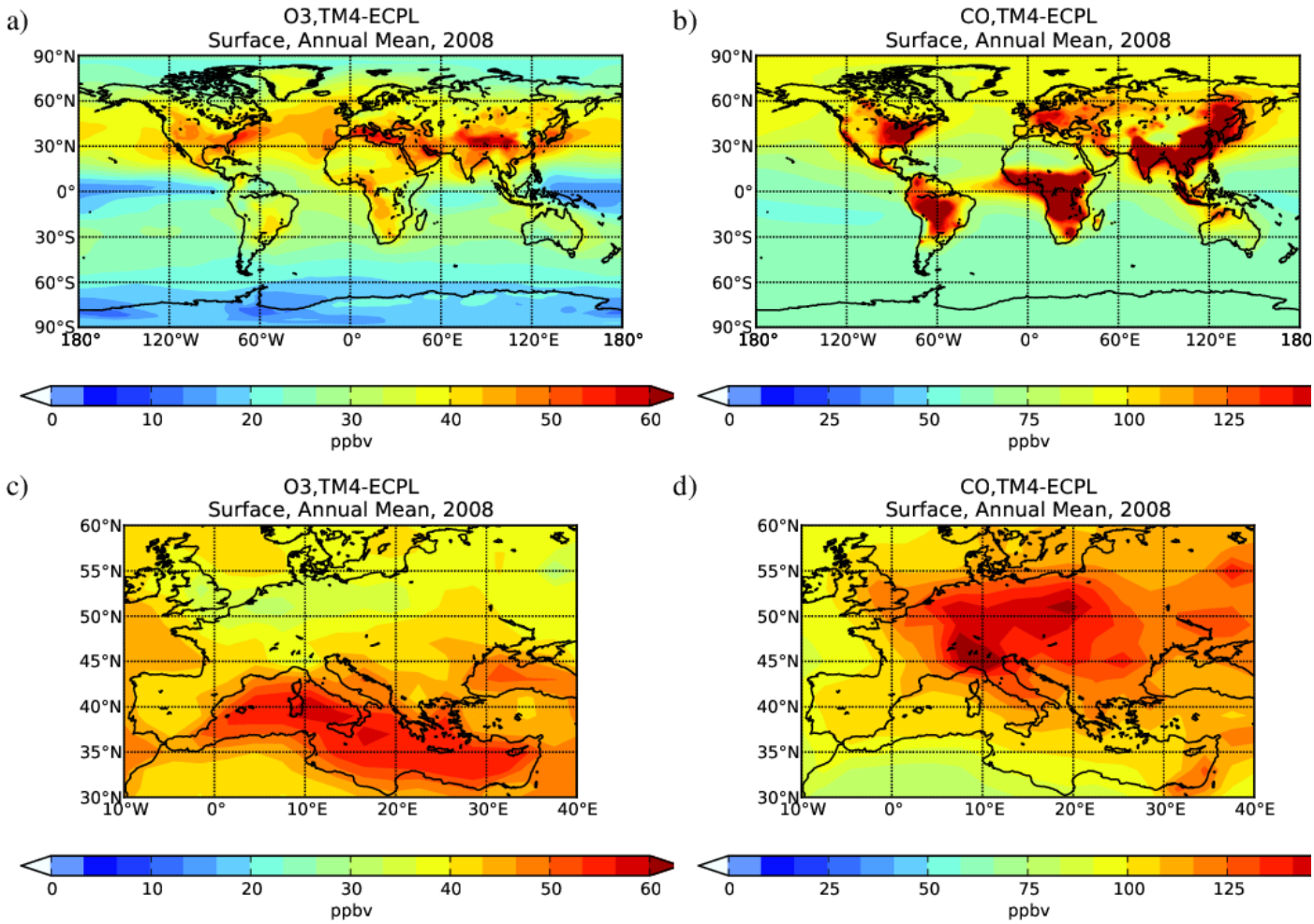

Fig. 7. Simulated a,c) O_3 and b,d) CO surface concentrations (ppb_v) for TM4-ECPL BASE simulation for the globe (a,b) and focus on the Mediterranean area (c,d).

836

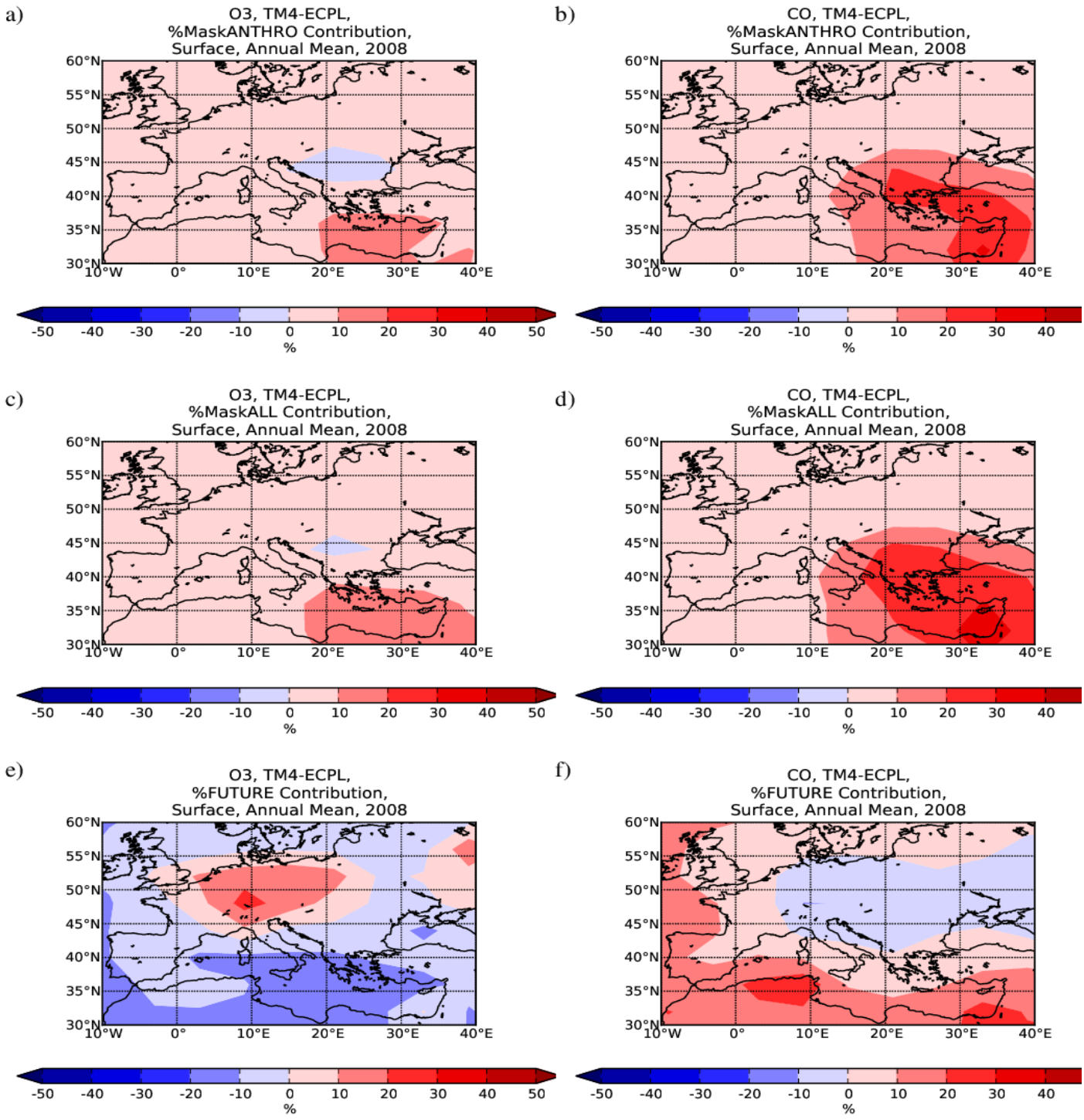

837

838 **Fig. 8.** Simulated relative contribution (%) to O_3 (left panels) and CO (right panels) surface
839 concentrations of a,b) Anthropogenic emissions over EM (MaskANTHRO); c,d) All emissions
840 over the EM (MaskALL); and e,f) Future anthropogenic emissions (FUTURE), compared to the
841 TM4-ECPL BASE simulation (figures a) through d) are computed as [100*(BASE-
842 MaskX)/BASE]; where MaskX is the respective sensitivity simulation, while e) and f) are
843 computed as [100x(FUTURE-BASE)/BASE]).

844